Fast-airflow tumble clothes dryer with small thermoelectric heat pump: Experimental evaluation

Philip Boudreaux,[a*] Chris Hall,[a] Kyle R. Gluesenkamp,[a] Steve Karman,[a] Jonathan Willocks,[a] Viral Patel,[a] Anthony Gehl[a]

[a]Oak Ridge National Laboratory, 1 Bethel Valley Rd, Oak Ridge, TN 37830, United States

Keywords: Clothes drying, high flow, thermoelectric, heat pump, rated efficiency

Abstract

Residential clothes drying accounts for about 5% of the total residential-sector energy consumption in the United States. Most dryers use electric resistance heaters to dry clothes and have low efficiencies. Higher-efficiency dryers that use vapor compression heat pumps are expensive and complex and have not gained a large market share in the United States. A novel tumble clothes dryer using a small thermoelectric heat pump with faster airflow than typical dryers is presented in this work. The benchtop performance of the thermoelectric heat pump and high-speed blower are presented, and the development of the prototype dryer is described. The dryer was tested for efficiency and dry time for a range of airflow rates and applied currents to the thermoelectric heat pump. The combined efficiency factor was 5.09–6.29 lb_{BDW}/kWh (specific moisture extraction rate of 1.23–1.53 kg_w/kWh) with 100–138 min dry times for these tests. The measured efficiency was 36%–68% greater than the minimum efficiency standard in the United States, and compared with vapor compression heat pump–based clothes dryers, the prototype dryer had less expensive, less complex components and did not use refrigerants. The performance of this small thermoelectric heat pump clothes dryer is also compared with previous iterations of the thermoelectric tumble clothes dryer described in the literature.

1. Introduction

Residential clothes drying in the United States consumes 192 TWh/year (657 TBtu/year) of primary energy, about 5% of the total residential-sector energy consumption, and contributes 22.7 billion metric tons of CO_2 emissions per year [1]. To measure dryer efficiency, the combined energy factor (CEF) is typically used in the United States. The CEF is the ratio of the bone-dry weight of the load in pounds to the energy needed to dry the load in kilowatt-hours. In other parts of the world, the specific moisture extraction rate (SMER) is used. The SMER is the ratio of water mass removed from the load in kilograms to the energy required to dry the load in kilowatt-hours. Both measures of efficiency are used in this work and can be converted to each other using equations found in Gluesenkamp et al. [2]. In the United States, the minimum efficiency standard for a standard-size vented electric dryer is 3.73 lb_{BDW}/kWh, or 0.91 kg_w/kWh [3]. To meet ENERGY STAR standards, a standard vented electric dryer needs to have a CEF over 3.93 lb_{BDW}/kWh, or 0.95 kg_w/kWh [4].

Most dryers in the US market are electric resistance based and meet or slightly exceed current efficiency standards [5]. Characteristics of electric resistance–based dryers are presented in Table 1 [2, 6]. These

---

[1] Notice: This manuscript has been authored by UT-Battelle, LLC, under contract DE-AC05-00OR22725 with the US Department of Energy (DOE). The US government retains and the publisher, by accepting the article for publication, acknowledges that the US government retains a nonexclusive, paid-up, irrevocable, worldwide license to publish or reproduce the published form of this manuscript, or allow others to do so, for US government purposes. DOE will provide public access to these results of federally sponsored research in accordance with the DOE Public Access Plan (https://www.energy.gov/doe-public-access-plan).
*Corresponding author. E-mail address: boudreauxpr@ornl.gov.

dryers have large inefficient heater elements and CEFs of 2.54–3.99 lb_{BDW}/kWh (0.62–0.97 kg_{w}/kWh). Higher-efficiency electric dryers on the market use vapor compression heat pumps rather than electric resistance heaters and are typically ventless [5]. They have impressive efficiencies between 4.30 and 11.0 lb_{BDW}/kWh (1.04 and 2.67 kg_{w}/kWh) and have dry times under 80 min [5]. However, because of the added components, the average unit cost is $424 more than that of electric resistance–based dryers, which could contribute to the low US market adoption of vapor compression heat pump units [7]. Current research in heat pump clothes drying includes investigating lower–global warming potential (GWP) refrigerants for vapor compression–based units, combining clothes drying with other vapor compression heat pump–based building equipment to reduce costs, and investigating alternative heat-pumping mechanisms.

All vapor compression–based heat pumps use a working fluid, or refrigerant. Traditional refrigerants have high GWPs. Investigating drop-in refrigerant replacements that do not require equipment modification is of high interest. Cop et al. replaced R134a refrigerant with a mixture of R290/RE170 and found they had similar efficiencies, but the R290/RE170 mixture resulted in a shorter dry time than R134a [8]. In a separate study, Gataric and Lorbek used R450A as a drop-in replacement and found that the total energy consumption decreased, but the dry time increased [9]. Another study tested R744 and found that, with some hardware modifications, energy consumption was reduced by 7.2% compared with R134a with similar dry times [10]. Singh et al. used numerical simulations to test a wide range of low-GWP refrigerants as replacements for R134a and found that R152a may be the best substitute [11].

Another recent area of vapor compression heat pump clothes-drying research has involved integrating equipment for dual use to reduce equipment costs. Singh et al. investigated a combined clothes-drying and space-conditioning system and reported annual energy-bill savings of $309 [11]. Another study investigated the addition of an electric heater between the heat pump and drum to decrease dry times because long dry times and high first costs are hurdles to the adoption of heat pump clothes dryers in the United States [12]. TeGrotenhuis et al. also noted that higher first costs of heat pump clothes dryers limit their adoption in the United States [13].

Others have investigated the use of alternative heat-pumping mechanisms to dry clothes, such as using a thermoelectric (TE) heat pump. The TE, or Peltier–Seebeck, effect refers to the temperature difference that occurs when a voltage is applied across a thermocouple or to the voltage produced by a thermocouple exposed to a temperature difference [14]. Many of these thermocouples can be combined in series and sandwiched between two electrically insulative substrates to create a TE device, sometimes called a TE module, and can be used for heat pumping [15]. TE-based clothes drying can have a lower unit cost, over vapor-compression based heat pump dryers, because the TE heater can be installed as a drop-in replacement for the electric resistance heater in a standard dryer while also offering substantial efficiency improvements over electric resistance without high-GWP refrigerants.

The literature concerning adapting TE heat pumping for clothes drying is sparse. In a simulation, a closed-loop TE tumble dryer was determined to have performance between that of an electric resistance condensing dryer and a vapor compression heat pump dryer [16]. Liu et al. developed a closed-loop drying cabinet for clothes and found that the SMER varied throughout the cycle and depended on TE input power [17]. Previous work implementing a thermoelectric heat pump (TEHP) into tumble clothes dryers at the US Department of Energy's Oak Ridge National Laboratory is summarized in Table 1 [18, 19]. Table 1 compares the airflow rates, heating powers, efficiencies, and dry times of the

TEHP-based dryers, including the iteration presented in this paper, with those of typical electric resistance–based clothes dryers.

Table 1. Configurations and performance for previous and current versions of the TEHP-based clothes dryer[a]

Dryer configuration	System illustration	Airflow rate, m^3/s (ft^3/min)	Heating power, W	Experimentally measured efficiency		Dry time for 3.83 kg (8.45 lb) load, min
				CEF, lb_{BDW}/kWh	SMER, kg_w/kWh	
Baseline electric resistance dryer [2, 6]	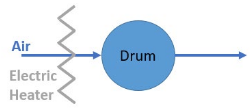	0.06 (120)	4,500	2.54–3.99	0.62–0.97	22–40
Prior work: TEHP—air based [18] (First-TED)	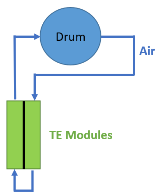	0.06 (123)	NR	5.26–6.51	1.33–1.64	100–159
Prior work: TEHP—pumped water loop with water-to-air HXs [19] (Pumped-TED)	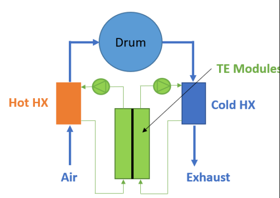	0.08 (165)	900	4.47–6.89	1.09–1.71	65–84
This work: TEHP—air based, vented (Fast-TED)	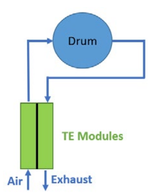	0.09 (193)	680	5.06–6.28	1.30–1.61	100–138

[a]HX = heat exchanger, NR = not reported in this paper

The first iteration of the TEHP tumble clothes dryer was a vented, or open-loop, design with 36 TE unit engines, which each comprised four TE modules fastened between two extruded aluminum heat sinks to transfer heat to the air [18]. Each TE module had 51 couples, for a total of 7344 couples. The TE unit engines were combined in a 6 × 6 grid, where ambient air entered a blower and directed air over the hot side of the TEHP and into the drum [18]. After the air exited the drum, it entered the cold side of the TEHP and then exited the dryer. Efficiencies between 5.26 and 6.51 lb_{BDW}/kWh (1.33 and 1.64 kg_w/kWh) were achieved during experimental testing of this heat sink–based TEHP dryer [18]. This version is referred to as First-TED in this paper.

The second iteration of the TEHP tumble dryer had a vented design and had only 30 TE modules, each with 127 Bi_2Te_3 couples, for a total of 3810 couples. Instead of using heat sinks to heat air, secondary pumped water loops transferred heat from the TE modules to the air using fin-and-tube heat exchangers on both the hot and cold sides of the TEHP [19]. Experimental trials showed efficiencies between 4.47 and 6.89 lb_{BDW}/kWh (1.09 and 1.71 kg_w/kWh) [19]. The maximum efficiency achieved with the secondary pumped loop prototype was 6% higher than that of First-TED with a shorter dry time. This was achieved with a smaller TEHP with fewer TE couples; however, system complexity increased with the secondary pumped loop. The second iteration is hereafter referred to as Pumped-TED.

A third iteration of the TEHP tumble clothes dryer, a fast-airflow TE clothes dryer called Fast-TED, is presented in this work, with a goal of reducing the TEHP costs and complexities of First-TED and Pumped-TED and the long dry times of First-TED. Fast-TED had a smaller-capacity TEHP with only 6 TE modules, the same models as used in Pumped-TED, and adopted the same heat sink–to–air heat transfer mechanism as First-TED. A total of 762 couples were contained in Fast-TED's TEHP. The low-capacity TEHP required less heat sink mass (approximately 16% of First-TED) and fewer TE couples, which would lead to substantial cost savings. To help improve the dry times of First-TED, an efficient high-speed blower was used to increase airflow through the drum. According to Shen et al., as airflow through the drum increases, dry time decreases [20]. To help decrease the pressure difference through the airflow path, which increases with high airflow rates, the rear duct bringing air from the hot side of the TEHP to the drum was redesigned and tested on the prototype.

This paper discusses the development and benchtop testing of the TEHP, high-speed blower performance, and impact of the redesigned rear duct. The Fast-TED prototype was fabricated and tested for efficiency and dry time, and the results are reported. Detailed air state point measurements for temperature, humidity, and pressure are presented and discussed. A summary of the prototype's performance is shown in Table 1 for comparison with electric resistance clothes dryers and First-TED and Pumped-TED.

2. Prototype development

To develop Fast-TED, a Samsung DV50K7500E 0.21 m^3 (7.5 ft^3) dryer was heavily modified. The rated CEF of this dryer before modification was 3.94 lb_{BDW}/kWh (0.96 kg_w/kWh) with a dry time of 65 min [21]. The original equipment (OE) air heater, rear duct connecting the heater and drum, and blower were replaced. These modifications were driven by previously published modeling [22].

2.1 Thermoelectric heat pump

The 5300W stock electric resistance heater was replaced with a small TEHP. The TEHP comprised six Thermonamic TEHC1-12708 TE modules, 40 mm by 40 mm in size, with 127 thermocouples each. Each TE module was sandwiched between two plate-fin aluminum heat sinks in a TE assembly as shown in Fig. 1(a). The heat sinks, TE module, and aluminum spacer block were all thermally connected by a thin layer of thermal paste. The six TE assemblies were then combined in a 2 × 3 grid and electrically connected in series as shown in Fig. 1(b).

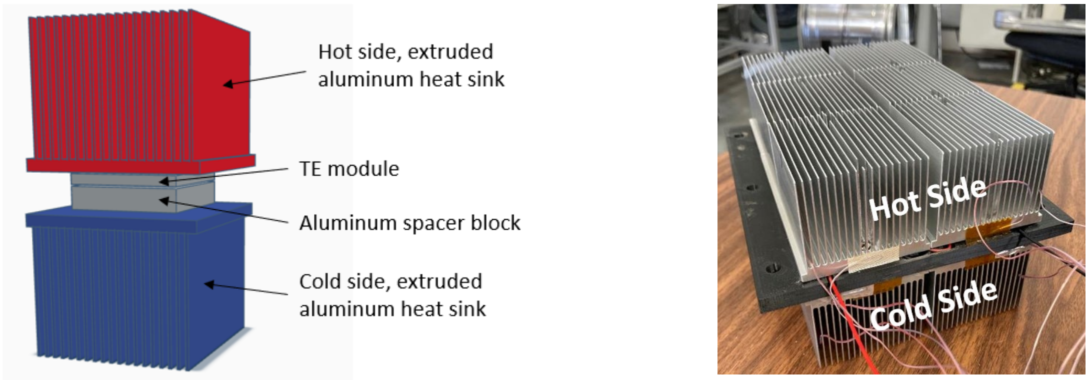

(a) (b)

Fig. 1. (a) TE assembly: TE modules sandwiched between two aluminum heat sinks. (b) Six TE assemblies combined to create the TEHP.

The TEHP was installed inside a 3D-printed enclosure with takeoffs for duct connections as shown in Fig. 2. The TEHP was performance tested outside of the dryer with a counterflow air path as shown in Fig. 2. A blower was connected to the inlet of the cold side to provide airflow.

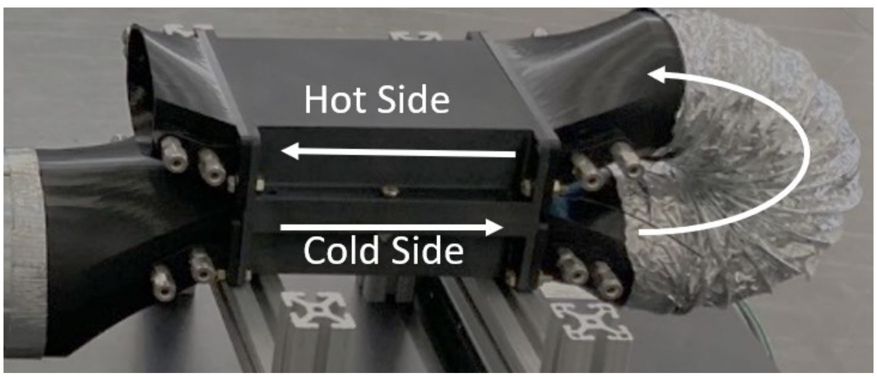

Fig. 2. Thermoelectric heat pump installed in a 3D-printed enclosure with duct takeoffs. Arrows show the direction of airflow for the benchtop test; the heat pump was tested in the counterflow orientation.

The TE modules were powered with an Ametek Sorensen XG-850 150-5.6 power supply at a constant direct current (DC) for each trial. An ebm-papst G3G225-RI07-01 variable-speed blower was used to provide airflow through the TEHP. The volumetric flow rates, air temperatures, heat sink temperatures, voltages and currents applied to the TEHP, and pressures were measured during tests using a National Instruments–based data acquisition system and LabVIEW virtual instrument. The measurement sensors and uncertainties are shown in Table 2, and sensor locations are shown in Fig. 3. The air temperature was measured at the inlet and outlet of both the cold and hot side of the TEHP with Resistance Temperature Detectors (RTD) with the measurement locations noted in Fig. 3. The temperature of each of the 12 aluminum heat sinks was measured with adhesive T-Type thermocouples (TC), also shown labeled in Fig. 3. Only six locations are shown in the figure. The other six heat sink temperature measurements are on the backside of the figure.

Table 2. Measurement instruments used for a benchtop TEHP test and their ranges and accuracies.

Measurement	Sensor	Range	Uncertainty
Flow rate	Air Monitor Aluminum LO-flo Pitot Traverse Station with Setra Model 264 pressure transducer	0.04–0.45 m^3/s	±2% of actual flow
Air temperature	Omega P-M-1/10-1/8-6-0-T-3 (1/10 DIN resistance temperature detector)	0°C–100°C	±0.06°C @ 40°C
Heat sink temperature	Omega 5TC-TT-T-30-36 (thermocouple)	−200°C–200°C	±1°C
Differential pressure	Setra Model 264 -1005WD11T1C	0–1,244 Pa	±7.5 Pa
TE power and current	AMETEK Sorensen XG-850 analog output voltage and current monitor	0–5.6 A 0–150 V	±0.056 A ±1.5 V

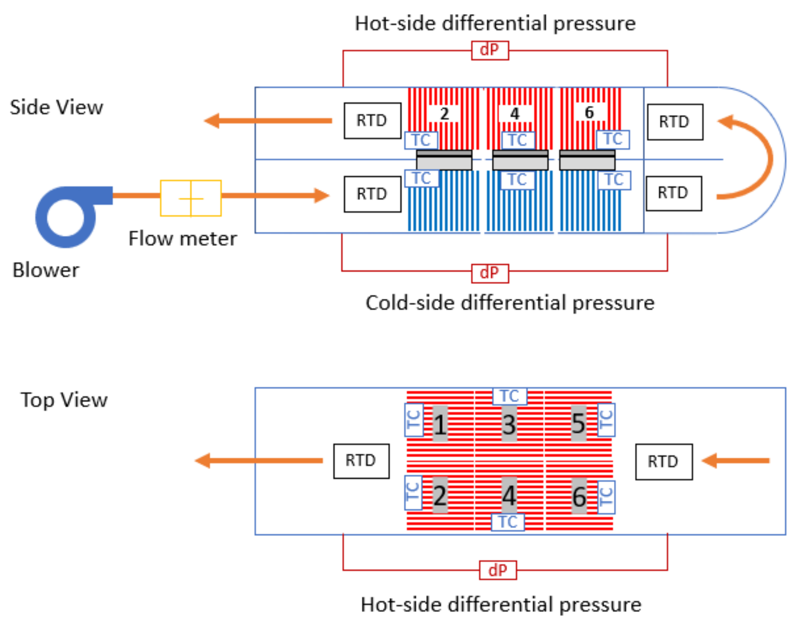

Fig. 3. Sensor locations for TEHP benchtop testing. Heat sinks are labeled numerically. RTD notes the location of all the resistive temperature detectors and TC notes the location of all the thermocouples.

Steady-state measurements were taken of the TEHP's performance at four blower speeds ranging from 0.046 to 0.096 m^3/s and four TE currents ranging from 3 to 5.6 A. Fig. 4 shows key temperature measurements on the hot side of the TEHP. Referring to Fig. 3, the heat sink temperature on the hot-side inlet was an average of the temperatures of the thermocouples attached to heat sinks 5 and 6. The outlet heat sink temperature was the average of the thermocouple temperatures on heat sinks 1 and 2. Note that the air-side temperature lifts increased with TE current and decreased with airflow rate. At a typical tumble dryer airflow of 0.066 m^3/s, the max temperature lift at a TE current of 5.6 A was 8.3°C. For comparison, First-TED had a temperature lift of about 15°C for a similar airflow rate [18].

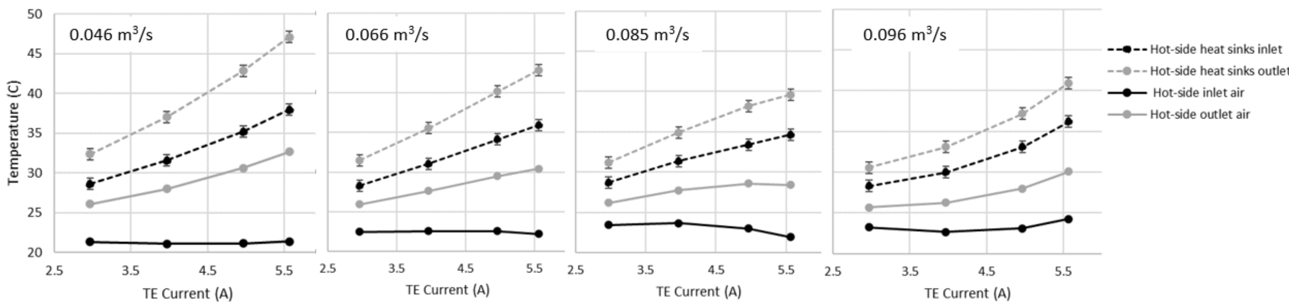

Fig. 4. Heat-sink and air temperatures at the inlet and outlet of the hot side of the TEHP as a function of TE current and airflow rate. Measurement uncertainty is shown as described in Table 3.

The hot-side heat transfer rate, $\dot{Q}_h$, and coefficient of performance, COP_h, were calculated using Eqs. (1) and (2), respectively. In Eq. (1), $\dot{m}$ is the mass flow rate of air, C_p is the specific heat capacity of air, and $T_{air,o}$ and $T_{air,i}$ are the outlet and inlet air temperatures, respectively, on the hot side of the TEHP. In Eq. (2), $P_{TEHP,AC}$ is the DC power applied to the TEHP divided by 0.9, which is the assumed efficiency of the alternating current (AC) to DC conversion.

$$\dot{Q}_h[W] = \dot{m}\,[\tfrac{kg}{s}] \cdot C_p[\tfrac{J}{kg\cdot K}] \cdot (T_{air,o}[K] - T_{air,i}\,[K]) \tag{1}$$

$$COP_h[-] = \frac{\dot{Q}_h[W]}{P_{TEHP,AC}[W]} \tag{2}$$

Fig. 5(a) shows the hot-side heat transfer and coefficient of performance of the TEHP as a function of TE current at a single flow rate of 0.096 m^3/s where error bars are displayed based on the propagation of uncertainties from Table 2 through Eqs. (1) and (2). Fig. 5(b) shows the total pressure differential across the hot and cold sides of the TEHP as a function of flow rate.

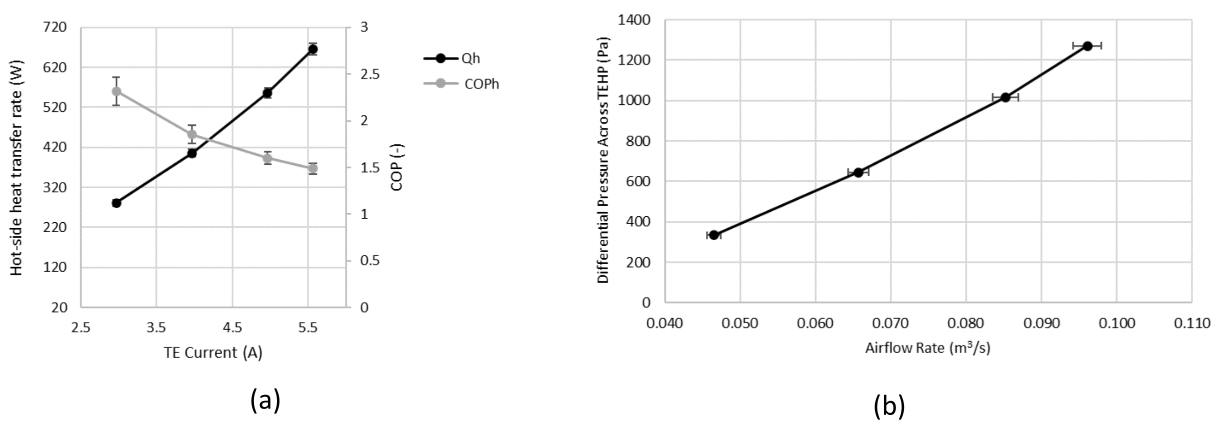

Fig. 5. (a) Hot-side heat transfer rate, $\dot{Q}_h$, and coefficient of performance, COP_h, of the TEHP at a flow rate of 0.096 m^3/s as a function of TE current; (b) differential pressure across both the cold and hot sides of the TEHP as a function of airflow rate.

2.2 High-efficiency, high-flow blower

A variable-speed, high-efficiency ebm-papst blower (G3G225RI0701) was used to replace the OE blower in the Samsung DV50K7500E clothes dryer. The OE impeller was removed from the motor arbor of the dryer so that only the high-speed blower was providing flow. The suction of the blower was connected to the exhaust of the dryer so that the blower was on the outside of the dryer cabinet. To characterize the dryer airflow path before the TEHP and rear duct were installed, the pressure differentials at the inlet and exhaust of the dryer were measured relative to ambient pressure. flow was measured at the blower exhaust, and blower power was measured as a function of blower speed. The sensor type, range, and uncertainty for these measurements are provided in Table 3.

Table 3. Measurements, sensors, sensor specifications for characterizing the dryer airflow path at high airflow rates.

Measurement	Sensor	Range	Uncertainty
Flow rate	Air Monitor Aluminum LO-flo Pitot Traverse Station with Setra Model 264 pressure transducer	0.04–0.45 m^3/s	±2% of actual flow
Blower power	Ohio Semitronics AC watt transducer (GW5-002C)	0–1,000 W	0.4 W
Differential pressure at dryer inlet	Setra Model 264-1003WD11T1C	0–747 Pa	± 7 Pa
Differential pressure at dryer exhaust	Setra Model 264-1010WD11T1C	0–2,488 Pa	±25 Pa

Fig. 6 shows the total pressure difference between the dryer inlet and exhaust and the blower power for flow rates ranging from 0.02 to 0.15 m^3/s. Note that at a typical tumble dryer airflow rate (0.066 m^3/s), blower power was less than 50 W with a total pressure difference of about 400 Pa between the air inlet and outlet. This illustrates the high efficiency of the blower. After the TEHP is installed, the system pressure is expected to rise significantly because, as shown in Fig. 5(a), at 0.066 m^3/s the TEHP had a total pressure difference of 650 Pa between the inlet and outlet. At higher flow rates, the pressure will increase further.

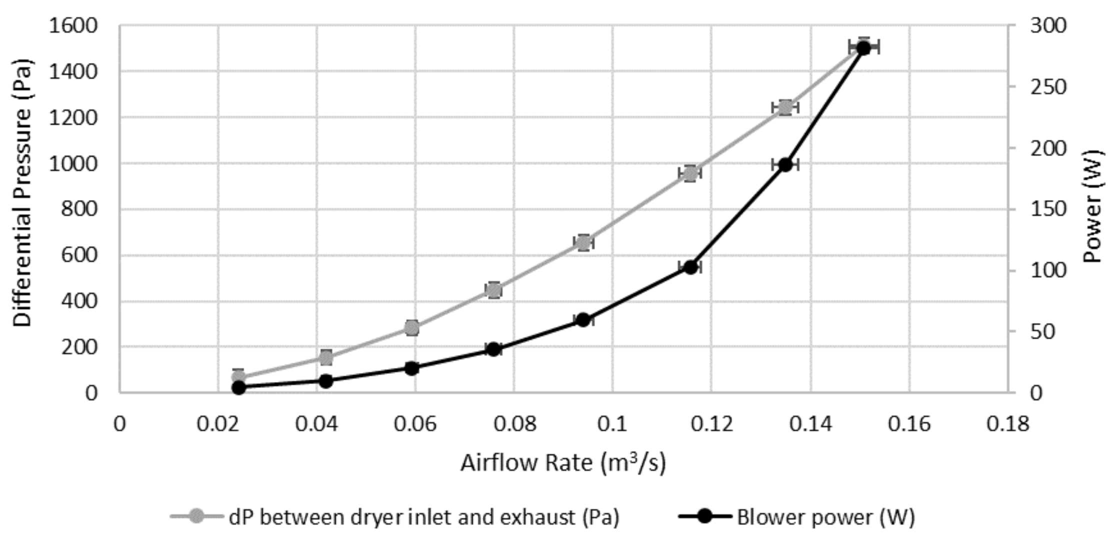

Fig 6. Differential pressure (dP) across the entire airflow path and blower power as a function of airflow rate after the high-speed blower was tested on the stock dryer without the original impeller installed. Measurement uncertainty is shown as described in Table 3.

2.3 Rear duct connecting TEHP outlet to drum inlet

Previous computational fluid dynamics modeling has shown that in the dryer airflow path, the rear duct that connects the air heater to the drum inlet could be redesigned to decrease the pressure drop through the airflow path [23]. The modeled performance of the optimized rear duct predicted that the total pressure drop through the airflow path could be reduced by 20% [23]. Because a highly restrictive TEHP was added to the airflow path and the dryer was run at a high airflow rate, decreasing the air resistance of other dryer components was critical in reducing the needed blower power to move air through the airflow path. A 3D-printed rear duct was fabricated based on the previous modeling study and installed in the dryer as shown in Fig. 7.

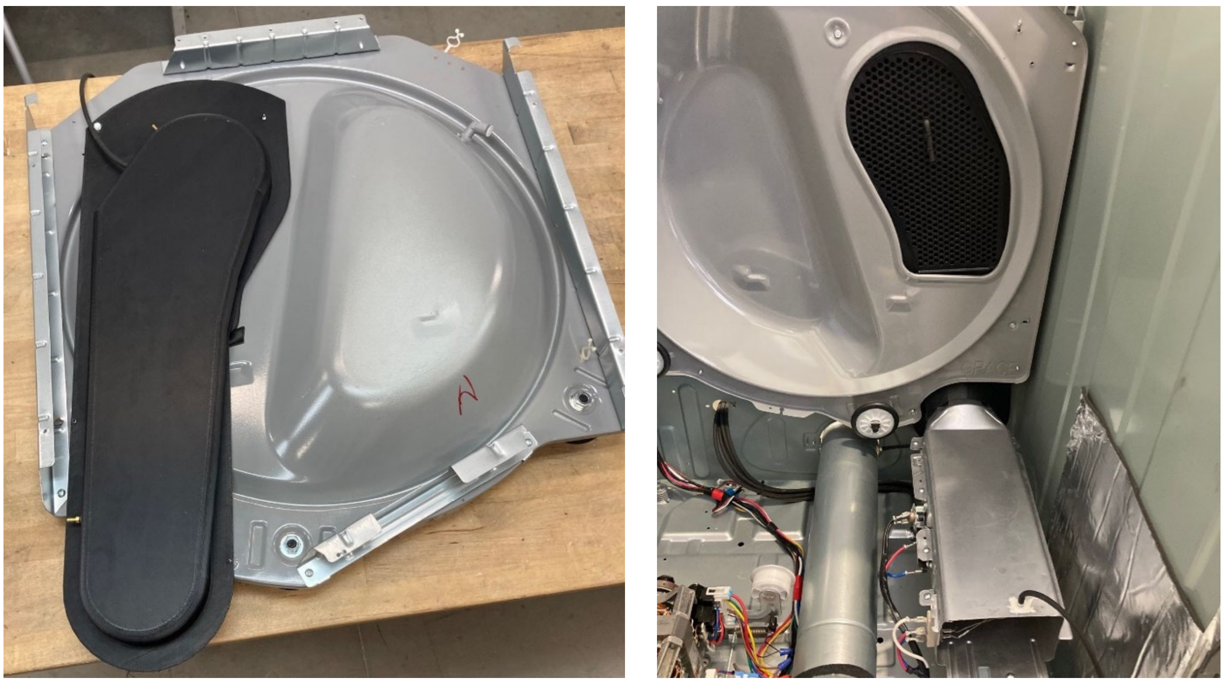

Fig. 7. Optimized rear duct to reduce the total airflow path pressure drop.

Once the rear duct was installed, the dryer was reassembled, and the duct pressure as a function of airflow rate was retested as described in Section 2.2. For this test, the TEHP was not installed, and the drum was empty and not rotating. Fig. 8 shows the comparison of the pressure drop along the airflow path between the OE and modified rear duct. At a typical dryer airflow rate of 0.066 m^3/s, the total pressure drop was indeed reduced by 20%, but as the flow rate increased, this percentage decreased.

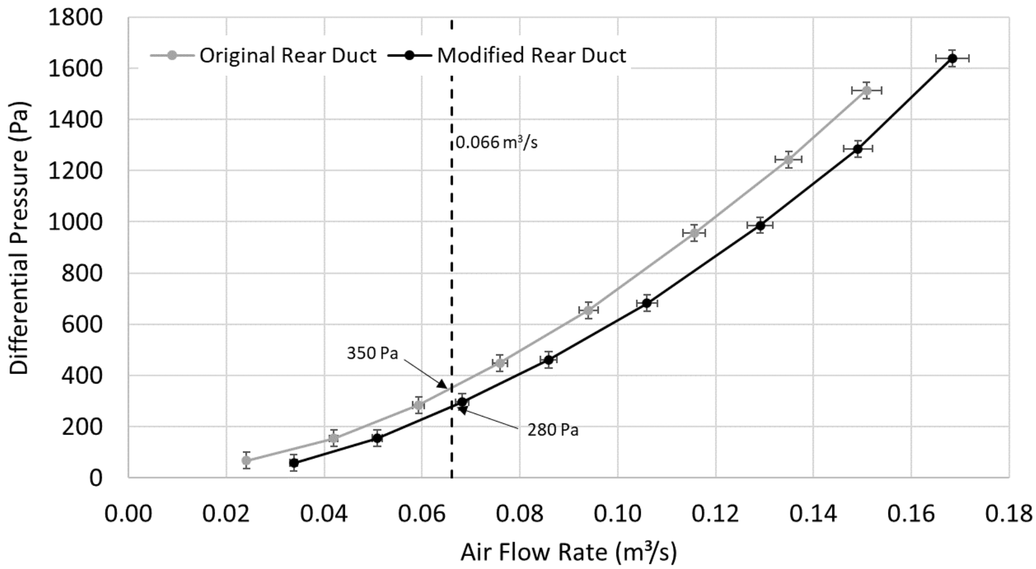

Fig. 8. Airflow-path pressure drop reduction after a 3D-printed optimized rear duct was installed with measurement uncertainty as shown in Table 3.

2.4 Full prototype

To build the Fast-TED prototype dryer, the OE motor that turned the drum and impeller, the electric resistance heater, and all electronic controls were removed from the donor dryer. A Midwest Motion MMP D33-655D-24V DC motor was installed in place of the OE motor to rotate the drum. The flow path was modified, and its components are listed here in order from the air inlet to the dryer exhaust as shown in Fig. 9: (1) hot side of the TEHPE, (2) optimized rear duct, (3) drum, (4) lint filter, (5) front duct, (6) cold side of the TEHP, and (7) high-efficiency blower. In this configuration, the TEHP was in a parallel-flow orientation instead of a counterflow orientation as tested on the bench described earlier. This configuration was chosen to simplify the air ducting. Air pressure, temperature, and relative humidity (RH) were measured along the airflow path at the air inlet (M1), the drum inlet (M2), the drum outlet (M3), and the TEHP cold-side outlet (M4) as shown in Fig. 9 using Setra differential pressure transducers and Vaisala Indigo520 TMP1 and HMP3 sensors, respectively. Power was measured separately for the TEHP, drum rotation motor, and blower. Airflow rate was measured at the exhaust of the blower, whose suction port was connected to the dryer exhaust. The TEHP was instrumented similarly to the benchtop test, with RTDs measuring air temperatures and thermocouples measuring heat sink surface temperatures. Table 4 shows all measurement instruments installed on the prototype dryer with locations, ranges, and uncertainties.

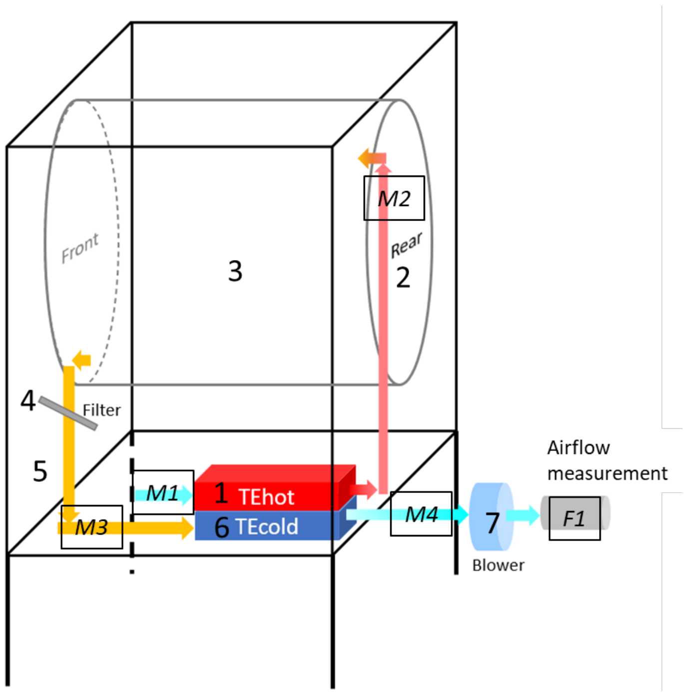

Fig. 9. Schematic of the Fast-TED prototype with the main components and air state point measurement locations labeled.

Table 4. Measurement locations with sensor types and accuracies for fully instrumented Fast-TED.

Measurement location[a]	Description	Unit	Range	Uncertainty (±)	Transducer manufacturer/ model/sensor
M1	TEHP inlet temperature	°C	−70–180	0.137 @23°C	Vaisala Indigo520—TMP1
M2	Drum inlet temperature				
M3	Filter outlet temperature				
M4	TEHP outlet temperature				
M1	TEHP inlet RH	% RH	0–100	0.8	Vaisala Indigo520—HMP3
M2	Drum inlet RH				
M3	Filter outlet RH				
M4	TEHP outlet RH				
M1	TEHP inlet pressure	Pa	0–747	7	Setra 264-1003WD11T1C
M2	Drum inlet pressure	Pa	0–747	7	Setra 264-1003WD11T1C
M3	Filter outlet pressure	Pa	0–1,244	12	Setra 264-1005WD11T1C
M4	TEHP outlet pressure	Pa	0–2,488	25	Setra 264-1010WD11T1C
F1	Flow at blower outlet	Pa	0–62	0.6	Setra 264-1R25WD11T1C
—	TE voltage	V	0–150	1.5	Sorensen XG 150-5
—	TE current	A	0–5.4	0.054	Sorensen XG 150-5
—	Blower power	W	0–1,000	0.4	Ohio Semitronics Watt Transducer GW5-002C
—	Drum rotator power	W	0–1,000	5	Ohio Semitronics Watt Transducer PC5-010DY25

TEHP	TEHP hot-side entering-air temperature	°C	0–100	0.06 @50°C	Omega P-M-1/10-1/8-6-0-T-3
TEHP	TEHP hot-side exiting-air temperature				
TEHP	TEHP cold-side entering-air temperature				
TEHP	TEHP cold-side exiting-air temperature				
TEHP	TE 1—hot-side heat sink temperature	°C	−200–200	1.4	Omega SA3-T (T-type TC)
TEHP	TE 2—hot-side heat sink temperature				
TEHP	TE 5—hot-side heat sink temperature				
TEHP	TE 6—hot-side heat sink temperature				
TEHP	TE 1—cold-side heat sink temperature				
TEHP	TE 2—cold-side heat sink temperature				
TEHP	TE 5—cold-side heat sink temperature				
TEHP	TE 6—cold-side heat sink temperature				
Dryer	Whole Dryer Scale	lb (kg)	0-500 (0-300)	0.05 (50)	Mettler Toledo 2158 MT 500LB 30X30 5KD
Test Load	Test Load Scale	g	0-27,000	2	Sartorius Midrics 1

[a]Refer to Fig. 9 for measurement locations along the dryer airflow path and Fig. 3 for measurement locations on the TEHP.

3. Testing methodology

Fast-TED dryer performance was tested in accordance with Title 10 of the *Code of Federal Regulations* (CFR), Appendix D1 to Subpart B of Part 430 [24], to determine the CEF and dry time for a standard 8.45 lb (3.83 kg) load with 57.5% starting moisture content. The test load was prepared according to the CFR using standard cloth and brought to the code-specified starting moisture content using a standard clothes washer [24]. To determine the bone-dry weight of the load as well as the mass of water added a Sartorius Midrics 1 scale was used. Fig. 10 shows the prototype dryer in an environmental chamber that was maintained at 22.2°C–25.6°C and 40%–60% relative humidity for all tests. The dryer was placed on a scale to monitor the whole dryer mass in real time throughout the dry cycle. When the drying cycle began, the data acquisition system recorded measurements from the sensors described in Table 4 at a resolution of 1 Hz. When the load reached 4% remaining moisture content, determined by comparing the current mass with the starting mass measured by the large scale, the cycle was terminated. After termination, the data were analyzed to compute the main performance metric, CEF, as described in the CFR [24]. CEF was computed using Eq. (3), where $m_{dry\ cloth}$ is the bone-dry mass of the cloth load and E_{tot} is the total cycle energy consumption [24]. The total cycle energy consumption is shown in Eq. (4), where the average AC powers (in kilowatts) of the TEHP, $P_{TEHP,AC}$; the drum motor, $P_{drum\ motor}$; and the blower, P_{blower}, are summed and multiplied by the cycle time, t_{cycle}, in hours and then multiplied by the normalized moisture content reduction of the load through the cycle [24]. The last constant in Eq. (4) is the field use factor for dryers with automatic control systems as described in the *Code of Federal Regulations* [24]. Eqs. (5) and (6) describe the starting moisture content, *SMC*, and final moisture content, *FMC*, respectively [24]. Starting moisture content and final moisture content were used to calculate the total cycle energy consumption. The SMER is calculated according to Eq. (7).

$$CEF\ \left[\frac{lb}{kWh}\right] = \frac{m_{dry\ cloth}[lb]}{E_{tot}[kWh]} \tag{3}$$

$$E_{tot}[kWh] = \left(P_{TEHP,AC} + P_{drum\ motor} + P_{blower}\right)[kW] \cdot t_{cycle}[h] \cdot \left(\frac{53.5}{SMC - FMC}\right) \cdot 1.04 \tag{4}$$

$$SMC[\%] = \frac{m_{water,initial}}{m_{dry\ cloth}} \cdot 100 \tag{5}$$

$$FMC[\%] = \frac{m_{water,final}}{m_{dry\ cloth}} \cdot 100 \tag{6}$$

$$SMER\left[\frac{kg_w}{kWh}\right] = \frac{m_{water,initial} - m_{water,final}}{E_{tot}} \tag{7}$$

Fig. 10. The completed dryer prototype in an environmental test chamber with the data acquisition computer cart on the left. The TEHP power supply, drum rotation motor power supply, and National Instruments cDAQ chassis used for data acquisition are underneath the dryer. The dryer sits on a large scale so that the load mass can be measured throughout the dry cycle.

4. Experimental results and discussion

The prototype was tested using loads with a starting moisture content of 57.5%, and trials were terminated when the load reached a final moisture content of 4%. A matrix of experimental trials with the blower operated at 70%, 80%, and 90% of the maximum speed and the TEHP operated at 4, 5, and 5.6 A was completed. Table 5 shows the performance results for each trial, including the CEF, calculated using Eq. (3), and the SMER calculated using Eq. (7). Uncertainty in CEF and SMER calculations are reported and are found by propagating the uncertainties in Table 4 through Eq. (3) and Eq. (7) respectively. Trial performance generally followed two trends as shown in Fig. 11. First, as the current applied to the TEHP increased, the CEF decreased, and the dry time decreased. Second, as the flow rate increased, the CEF decreased, and the dry time decreased. The most efficient trial (9) had the lowest flow rate and TE current. The fastest trial (1) had the highest flow rate and TE current.

Table 5. Dry-time and combined-energy-factor results of dryer cycle tests.

Trial	Blower speed (%)	TE current (A)	Average airflow rate (m^3/s)	Average DC TE power (W)	Average blower + drum motor power (W)	Dry time (min)	CEF (lb_{BDW}/kWh)	SMER (kg_w/kWh)
1	90	5.6	0.090	445.0	451.6	100.1	5.09±0.06	1.23±0.02
2	90	5	0.091	345.1	464.9	100.4	5.45±0.07	1.26±0.02
3	90	4	0.092	215.6	460.6	108.5	6.05±0.08	1.39±0.02
4	80	5.6	0.075	459.6	373.7	109.6	5.07±0.07	1.25±0.02
5	80	5	0.079	351.3	370.5	108	5.70±0.08	1.34±0.02
6	80	4	0.077	220.1	367.4	126	6.20±0.09	1.48±0.02
7	70	5.6	0.065	466.2	293.9	121.7	5.14±0.08	1.31±0.02
8	70	5	0.065	361.3	295.9	130.3	5.38±0.08	1.32±0.02
9	70	4	0.064	233.1	301.0	137.7	6.29±0.10	1.53±0.03

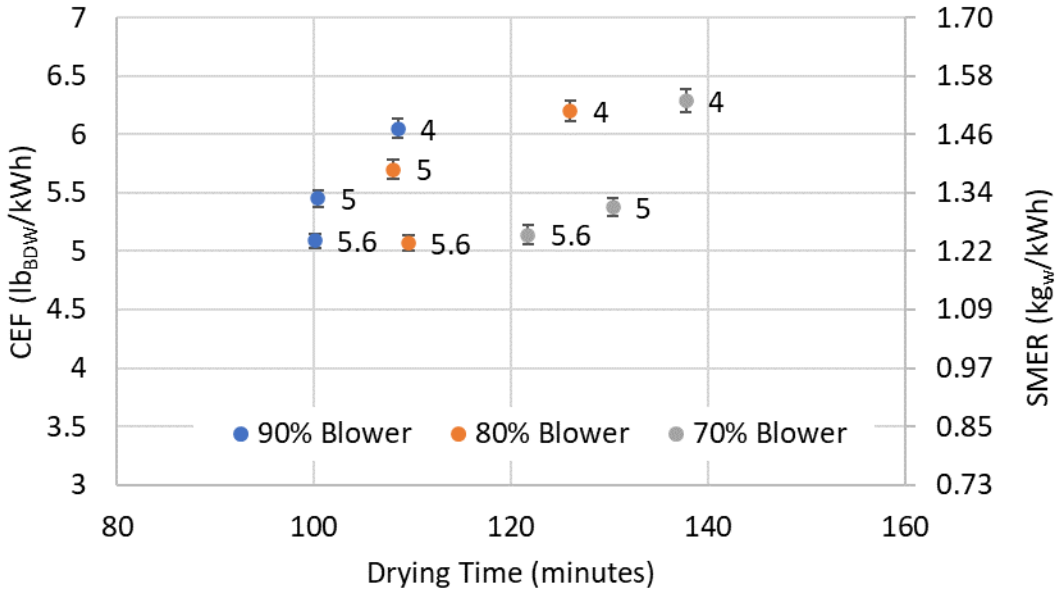

Figure 11: Thermoelectric clothes dryer efficiency performance for three different blower speeds and three different currents applied to the TEHP.

Fig. 12 compares the performance of the Fast-TED presented in this work with previous research, the ENERGY STAR criteria, and the CFR standard. Compared with the CFR standard, this dryer was between 36% and 68% more efficient depending on flow rate and TEHP power [3]. Compared with ENERGY STAR criteria, this dryer was 30% to 63% more efficient, but no trials had dry times under the ENERGY STAR requirement of 80 min [4]. Experimental trials in this work for Fast-TED were more efficient than most First-TED trials [18] and Pumped-TED [19] trials except for one outlier in each dataset. However, the dry time was similar to that of First-TED and much longer than that of Pumped-TED.

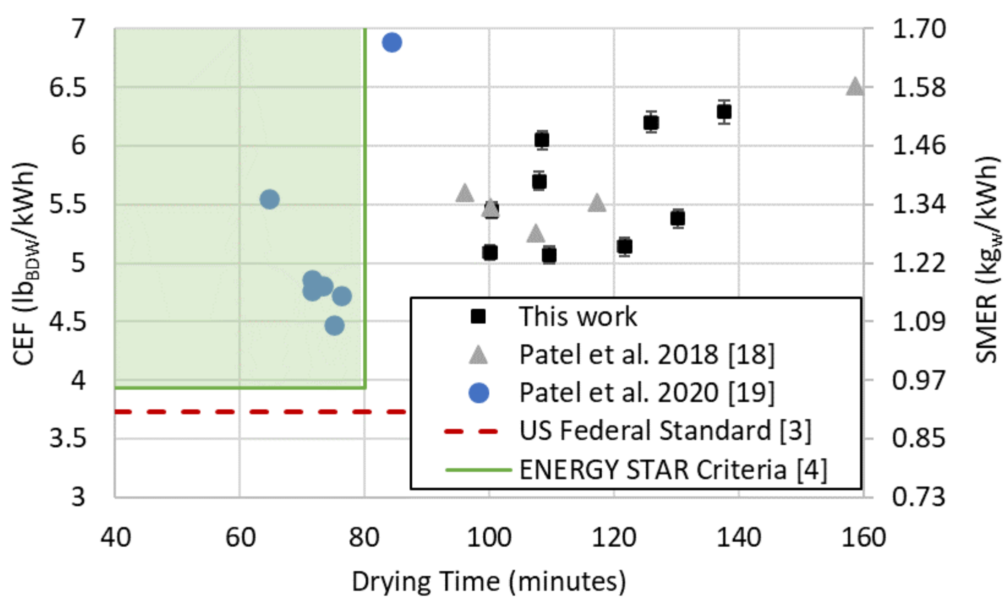

Fig. 12. Thermoelectric clothes dryer performance from this work compared with previous work [18] [19], the CFR standard [3], and ENERGY STAR performance criteria [4].

Fig. 13 shows the time-dependent power, TEHP heat transfer rates, air temperatures, and humidities for trial 1. Fig. 13(a) shows that the average TEHP AC power was 494.4 W, the blower power was 275.6 W, and the drum motor power was 175.6 W. The total average power consumption of the dryer was 945.6 W.

Fig. 13(b) shows the TEHP heat transfer rates; these rates were computed as described in Eq. (1). The airflow through the cold side of the TEHP was assumed to be equal to the flow rate through the fan. The airflow through the hot side of the TEHP was not measured directly but is known to be less than the flow rate through the cold side due to duct leakage to the ambient environment. To estimate the flow rate through the hot side of the TEHP, the hot-side flow was reduced from the flow measured at the blower until the energy balance of $\dot{Q}_c$ plus $P_{TEHP,AC}$ was equal to $\dot{Q}_h$. Using this procedure, the flow rate through the hot side of the TEHP for trial 1 was estimated to be 48% of the flow through the blower. This results in estimated average hot- and cold-side heat transfer rates of 722.5 and 231.7 W respectively and a COP_h of 1.47 and COP_c 0.47.

Fig. 13(c) and 13(b) show the air temperature and relative humidity at the state points described in Fig. 9. The drum inlet air temperature was 36°C during steady-state operation, so the TEHP provided a 12°C temperature lift compared with the hot-side inlet air temperature.

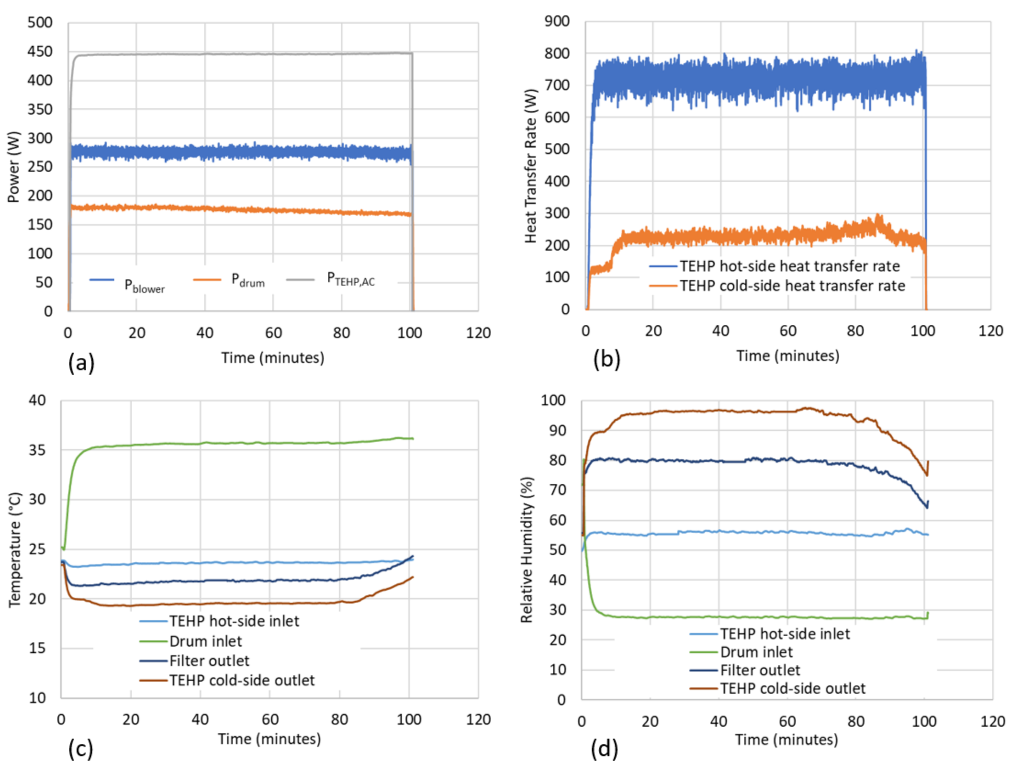

Fig. 13. Key measurements of trial 1 with a blower speed of 90% of the maximum and a TEHP current of 5.6 A: (a) AC power consumption of the blower, drum motor, and TEHP; (b) TEHP hot- and cold-side heat transfer rates; and (c) air temperature and (d) humidity for four state points along the airflow path.

4.1 Dryer drum effectiveness

This prototype employed a high-speed blower to povide a higher airflow rate than typical dryers to shorten dry time. Previous work has shown that the dryer drum effectiveness (DDE) of moisture transfer between the cloth and air is dependent on the airflow rate and drum inlet air temperature [25]. The DDE for mass transfer, ε_m, is defined by Eq. (9) and is a ratio of the measured mass or moisture transfer rate to the maximum-possible mass transfer rate, where ω_{in} is the humidity ratio of the air entering the drum, ω_{out} is the humidity ratio of the air exiting the drum, and ω_{surf} is the humidity ratio of the cloth surface assumed to be at saturation [26]. The DDEs for all nine trials of Fast-TED were calculated according to the procedure in Gluesenkamp et al. [26].

$$\varepsilon_m = \frac{(\omega_{out} - \omega_{in})}{(\omega_{surf} - \omega_{in})} \tag{9}$$

According to Gluesenkamp et al. [26], the DDE increases as the residence time or drum inlet temperature increases. The residence time, τ, is defined as the ratio of the drum volume, V_{drum}, to the airflow rate through the drum, $\dot{V}_{drum}$, as shown in Eq. (10). Table 7 shows the residence time and entering–drum air temperature for each trial shown in Table 5.

$$\tau = \frac{V_{drum}}{\dot{V}_{drum}} \tag{10}$$

The calculated DDEs for select trials are plotted in Fig. 15 as a function of remaining moisture content, *RMC*, which is the percent ratio of the mass of water, m_w, in the cloth load to the bone-dry mass of the load, m_{BDW}, as shown in Eq. (11). The cloth in the dryer started with a remaining moisture content of 57.5% and ended at 4%, so in Fig. 15, time increases from right to left.

$$RMC = 100 \cdot \frac{m_w}{m_{BDW}} \tag{11}$$

Fig. 14(a) shows the DDE as a function of the remaining moisture content for three trials with the same residence time but differing entering–drum air temperatures due to differing currents applied to the TEHP. As the drum inlet temperature increased, the DDE increased, as can be seen most clearly in the constant-rate drying period between 50% and 15% remaining moisture content.

Table 6. Residence times, entering–drum air temperatures, and dry times for all trials in Table 5.

Trial	Residence time (s)	Entering–drum air temperature (°C)	Dry time (min)
1	2.03	35.7	100.1
2	2.01	33.2	100.4
3	1.99	30.6	108.5
4	2.44	38.6	109.6
5	2.31	35.4	108
6	2.37	32.3	126
7	2.81	40.6	121.7
8	2.81	37.7	130.3
9	2.85	33.2	137.7

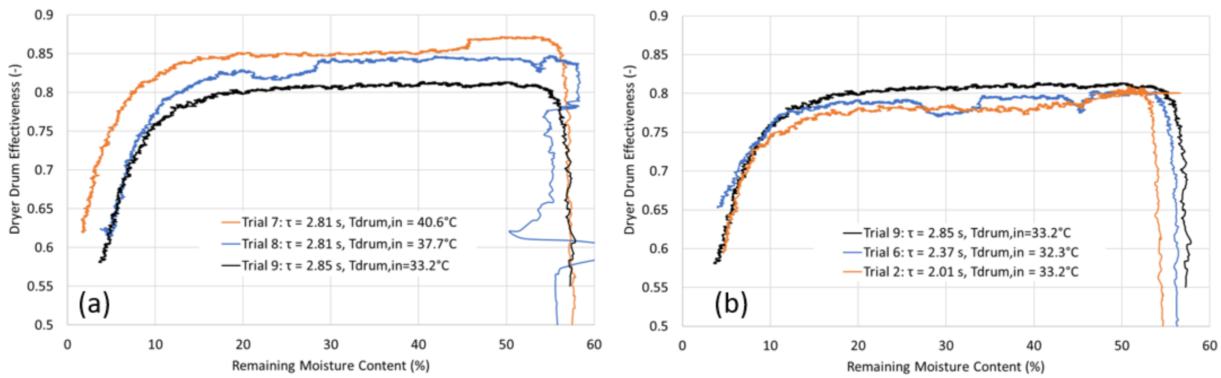

Fig. 14. DDE as a function of remaining moisture content through the dry cycle for select trials from Table 5 (a) with varying entering–drum air temperatures and (b) with varying residence times. Time increases from right to left.

Fig. 14(b) shows the DDEs for three trials with the same drum inlet air temperature but different residence times. In general, longer residence times resulted in higher DDEs during the constant-rate drying period of the cycle. These results confirm what was reported in Gluesenkamp et al. [26]: that a shorter residence time results in a lower DDE. Despite this lower DDE, the higher airflow rate resulted in a shorter dry time. Refering to Fig. 14(b) and Table 7, trial 2, which had the shortest residence time, had the shortest dry time (100.4 min). Trial 9, which had the longest residence time of the three trials plotted, had the longest dry time (137.7 min). This trend shows that even though faster airflow rates resulted in less efficient moisture transfer between the cloth and air, dry times were improved.

4.3 Limitations of this work

The same donor dryer was used in this work as was used in the Pumped-TED prototype, and similar DC drum motors were used to rotate the drum. However, for Pumped-TED, the drum motor required only 118 W to rotate the drum, but for Fast-TED, the drum motor required 180 W because of the high-volume optimized rear duct that was installed in the dryer. The duct was too deep and contacted the back wall of the dryer cabinet, and once assembled, the sliding seals on the drum were compressed and provided more friction than usual. This issue was not noticed until testing was completed. If a drum motor power of 118 W had been used, then the CEFs of all trials would have increased by 7%–14% depending on the trial dry time.

Another limitation of this work is that the actual airflow through the hot side of the TEHP was not measured during effeciency testing. Because the flow was not measured, the TEHP heat transfer rate and coefficient of performance were calculated based on adjusting the estimated flow through the hot side of the TEHP so get a favorable energy balance. This doesn't impact the reported efficiency of Fast-TED.

5. Conclusions

A prototype tumble clothes dryer with a fast airflow rate (40% higher than that of typical clothes dryers), low-capacity TEHP with only 6 TE modules, and redesigned rear duct optimized to reduce the total duct pressure was built and tested. The prototype dryer was tested at different airflow rates and TEHP powers. The most efficient trial had a CEF of 6.29 lb_{BDW}/kWh (SMER of 1.53 kg_w/kWh) with a dry time of

138 min. The fastest trial had a CEF of 5.09 lb_{BDW}/kWh (SMER of 1.23 kg_w/kWh) with a dry time of 100 min. Trials of this version of the TE clothes dryer were more efficient than most of the trials of the previous two versions [18,19] except for one outlier in each dataset. The dry time of this version was similar to the dry time of the first version of the TEHP dryer with a heat-sink-to-air based heat exchanger and was much longer than the dry time of the pumped water loop version. The unit cost of this new TEHP dryer is expected to be lower than that of previous versions because of the reduction in TE modules, aluminum heat sinks, and system complexity.

6. CRediT authorship contribution statement

Philip Boudreaux: Writing - Original Draft, Investigation, Software, Methodology, Visualization, Project Administration, Data Curation

Chris Hall: Writing – Original Draft, Software, Investigation, Visualization

Kyle R. Gluesenkamp: Funding Acquisition, Writing – Reviewing & Editing

Steve Karman: Software

Jonathan Willocks: Resources, Investigation

Viral Patel: Project Administration, Funding Acquisition, Investigation, Software, Methodology, Visualization

Anthony Gehl: Resources

7. Acknowledgements

This work was sponsored by the US Department of Energy's Building Technologies Office under Contract No. DE-AC05-00OR22725 with UT-Battelle LLC. The authors would like to acknowledge Dr. Wyatt Merrill, Technology Manager—Building Electric Appliances, Devices, and Systems (BEADS), US Department of Energy Building Technologies Office.

8. References

[1] US Department of Energy. Scout, https://scout.energy.gov/ [accessed 2023-06-07].

[2] Gluesenkamp KR, Patel VK, Momen AM (2020). Efficiency limits of evaporative fabric drying methods, Drying Technology, 39:1, 104-124, DOI: 10.1080/07373937.2020.1839486.

[3] 10 CFR 430, Title 10, Energy, Part 430, Energy conservation program for consumer products, Subpart C, Energy and water conservation standards, 2024, US Office of the Federal Register.

[4] ENERGY STAR, Energy star clothes dryer key product criteria, US Environmental Protection Agency and US Department of Energy, 2020, https://www.energystar.gov/products/appliances/clothes_dryers/key_product_criteria.

[5] US Environmental Protection Agency. ENERGY STAR certified residential clothes dryers, https://www.energystar.gov/productfinder/product/certified-clothes-dryers/results [accessed 2023-06-27].

[6] TeGrotenhuis W (2014). Clothes dryer automatic termination sensor evaluation: Volume 1: Characterization of energy use in residential clothes dryers, PNNL-23621, Pacific Northwest National Laboratory, Richland, WA.

[7] Graban A, Groll E, Braun J, Ziviani D (2021). Review of heat pump tumble clothes dryer energy efficiency and related technologies, International Refrigeration and Air Conditioning Conference, Paper 2222.

[8] Cop M, Barta RB, Thomas C, Hesse U (2024). Experimental investigation of a heat pump tumble dryer with a zeotropic refrigerant mixture, International Journal of Refrigeration, 158, 190-201, DOI: 10.1016/j.ijrefrig.2023.11.018.

[9] Gataric P, Lorbek K (2021). Evaluating R450A as a drop-in replacement for R134a in household heat pump tumble dryers, International Journal of Refrigeration, 128, 22-33. DOI: 10.1016/j.ijrefrig.2021.03.020.

[10] Brandt N, Alpogger T, Tegethoff W, Bockholt M, Mohlenkamp A, Kohler J (2019). Exergetic analysis of different R744 heat pump tumble dryer system topologies, Applied Thermal Engineering, 161, 114107.

[11] Singh A, Sarkar J, Sahoo RR (2020). Energetic and exergetic performance simulation of open-type heat pump dryer with next-generation refrigerants, Drying Technology, 38:8, 1011-1023.

[12] Singh A, Sarkar J, Sahoo RR (2022). Experimental investigation on novel heat pump system for combined drying and air conditioning for arid climate, Drying Technology, 40:16, 3556-3567.

[13] TeGrotenhuis WE, Butterfield A, Caldwell D, Crook A, Winkleman A (2017). Modeling and design of a high efficiency hybrid heat pump clothes dryer, Applied Thermal Engineering, 124, 170-177.

[14] Zoui MA, Bentouba S, Stocholm JG, Bourouis M (2020). A review on thermoelectric generators: Progress and applications, Energies, 13:14, 3606. DOI: 10.3390/en13143606.

[15] Das AK (2018). A review on thermoelectric effects and phenomenon, International Journal of Research in Engineering, IT and Social Sciences, 8:9, 242-247.

[16] Somdalen R, Kohler J (2018). Theoretical investigation of a novel thermoelectric laundry dryer concept, Materials Today: Proceedings, 5:4, 10323-10332.

[17] Liu D, Zhao F-Y, Tang G-F (2008). Modeling and performance investigation of a closed-type thermoelectric clothes dryer, Drying Technology, 26:10, 1208-1216, DOI: 10.1080/07373930802306995.

[18] Patel VK, Gluesenkamp KR, Goodman D, Gehl A (2018). Experimental evaluation and thermodynamic system modeling of thermoelectric heat pump clothes dryer, Applied Energy, 217, 221-232, DOI: 10.1016/j.apenergy.2018.02.055.

[19] Patel VK, Boudreaux PR, Gluesenkamp KR (2021). Validated model of a thermoelectric heat pump clothes dryer using secondary pumped loops, Applied Thermal Engineering, 184, 116345, DOI: 10.1016/j.applthermaleng.2020.116345.

[20] Shen B, Gluesenkamp K, Boudreaux PR, Patel VK (2018). Model-based air flow path optimization for heat pump clothes dryer, International Refrigeration and Air Conditioning Conference, Paper 1955, https://docs.lib.purdue.edu/iracc/1955.

[21] ENERGY STAR, Certified clothes dryer, details, https://www.energystar.gov/productfinder/product/certified-clothes-dryers/details-plus/2255002 [accessed 2024-06-01].

[22] Boudreaux P, Patel V, Hall C, Gluesenkamp K, Karman S, Ellis D, Gehl A (2022). Performance modeling of a thermoelectric heat pump clothes dryer with very high airflow, International Refrigeration and Air Conditioning Conference, Purdue University, July 1–14, 2022.

[23] Hall C, Karman S, Boudreaux P, Patel V, Ellis D (2022). CFD modeling of very high airflow in a residential clothes dryer to investigate pressure loss and flow through the airflow path, International Refrigeration and Air Conditioning Conference, Purdue University, July 1–14, 2022.

[24] 10 CFR 430, Title 10, Energy, Part 430, Energy conservation program for consumer products, Subpart B, Test procedures, Appendix D1, Uniform test method for measuring the energy consumption of clothes dryers, 2013, US Office of the Federal Register.

[25] Gluesenkamp KR, Boudreaux P, Patel VK, Goodman D, Shen B (2019). An efficient correlation for heat and mass transfer effectiveness in tumble-type clothes dryer drums, Energy, 172, 1225–1242, DOI: 10.1016/j.energy.2019.01.146.

Nomenclature

A	amperes
AC	alternating current
CEF	combined energy factor, lb_{BDW}/kWh
CFR	*Code of Federal Regulations*
COP	coefficient of performance
C_p	specific heat of air
C_v	leakage coefficient, $m^3/(s{\cdot}Pa^{0.5})$
DC	direct current
DDE	dryer drum effectiveness

dP	differential pressure between the dryer airflow path and the ambient, Pa
ε	dryer drum effectiveness
E_{tot}	total cycle energy, kWh
Fast-TED	fast-airflow thermoelectric clothes dryer
FMC	final moisture content
First-TED	first-iteration thermoelectric clothes dryer
GWP	global warming potential
HX	heat exchanger
Hz	hertz
kWh	kilowatt-hour
m	mass, kg
$\dot{m}$	mass flow rate of air, kg/s
NR	not reported
OE	original equipment
P	power, W
Pa	pascals
Pumped-TED	pumped loop thermoelectric clothes dryer
$\dot{Q}$	heat transfer rate, W
RH	relative humidity
RMC	remaining moisture content, %
RMS	Root-mean-squared
RTD	resistance temperature detector
SMC	starting moisture content
SMER	specific moisture extraction rate, kg_w/kWh
T	temperature, °C
t	time, s or min
τ	residence time, s
TBtu	trillion British thermal units
TC	thermocouple

TE	thermoelectric
TEHP	thermoelectric heat pump
TWh	terawatt-hour
V	volt
V_{drum}	volume of the dryer drum, m^3
$\dot{V}$	volumetric flow rate of air, m^3/s
ω	humidity ratio, $kg_{water}/kg_{dry\ air}$

Subscripts

AC	alternating current
air	air
BDW	bone-dry weight of cloth load
blower	blower used to move air through dryer airflow path
c	cold side
cycle	one complete dryer cycle to dry clothes from 57.5% to 4% moisture content
drum	dryer drum
drum motor	motor used to rotate drum
dry cloth	cloth with no moisture
final	state of water in the cloth at end of dry cycle
h	hot side
i	in
initial	state of water in the cloth at start of dry cycle
m	mass transfer referring to effectiveness
o	out
surf	saturated surface of cloth
TEHP	thermoelectric heat pump
w	water
water	water contained in the cloth